ACS APPLIED NANO MATERIALS

www.acsanm.org Article

Nanometer-Thick ZnO/SnO_2 Heterostructures Grown on Alumina for H_2S Sensing

Mehdi Akbari-Saatlu,* Marcin Procek, Claes Mattsson, Göran Thungström, Tobias Törndahl, Ben Li, Jiale Su, Wenjuan Xiong,* and Henry H. Radamson*

Cite This: *ACS Appl. Nano Mater.* 2022, 5, 6954–6963 Read Online

ACCESS | Metrics & More | Article Recommendations | Supporting Information

ABSTRACT: Designing heterostructure materials at the nanoscale is a well-known method to enhance gas sensing performance. In this study, a mixed solution of zinc chloride and tin (II) chloride dihydrate, dissolved in ethanol solvent, was used as the initial precursor for depositing the sensing layer on alumina substrates using the ultrasonic spray pyrolysis (USP) method. Several ZnO/SnO_2 heterostructures were grown by applying different ratios in the initial precursors. These heterostructures were used as active materials for the sensing of H_2S gas molecules. The results revealed that an increase in the zinc chloride in the USP precursor alters the H_2S sensitivity of the sensor. The optimal working temperature was found to be 450 °C. The sensor, containing 5:1 ($ZnCl_2$: $SnCl_2 \cdot 2H_2O$) ratio in the USP precursor, demonstrates a higher response than the pure SnO_2 (~95 times) sample and other heterostructures. Later, the selectivity of the ZnO/SnO_2 heterostructures toward 5 ppm NO_2, 200 ppm methanol, and 100 ppm of CH_4, acetone, and ethanol was also examined. The gas sensing mechanism of the ZnO/SnO_2 was analyzed and the remarkably enhanced gas-sensing performance was mainly attributed to the heterostructure formation between ZnO and SnO_2. The synthesized materials were also analyzed by X-ray diffraction, scanning electron microscopy, energy-dispersive X-ray, transmission electron microscopy, and X-ray photoelectron spectra to investigate the material distribution, grain size, and material quality of ZnO/SnO_2 heterostructures.

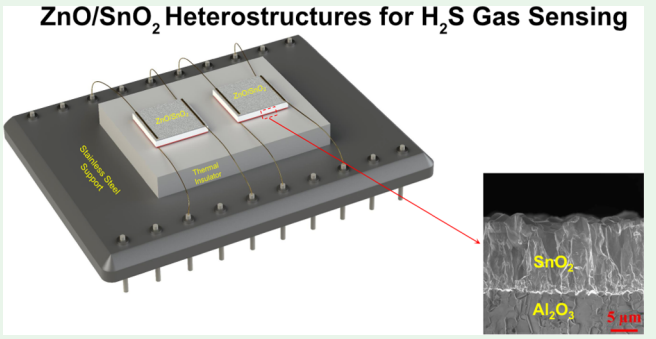

KEYWORDS: *gas sensors, ZnO/SnO_2, heterostructures, ultrasonic spray pyrolysis, H_2S*

Downloaded via UPPSALA UNIV on August 24, 2022 at 13:21:52 (UTC).
See https://pubs.acs.org/sharingguidelines for options on how to legitimately share published articles.

INTRODUCTION

It is well-known that metal oxide semiconductors are an excellent gas sensing material simply because of their high sensitivity to small concentrations of gases, long-term stability, low fabrication costs, and high potential to provide a small and low power-consuming sensor.[1−4] In order to improve the gas sensing performance of sensors containing a single metal oxide, many research works have been performed using the homojunction between grains to study the grain size effect and morphological influence on gas sensing.[5] However, due to the fact that the single metal oxides give an equal response to a wide range of gases, the selectivity of the sensor still remains a challenging issue.[6] Many efforts have been focused on improving metal oxides' selectivity by (a) doping with noble catalytic metals to promote the reaction to a specific gas, (b) surface modification, (c) using machine learning, and (d) use of multicompositional sensing films.[7,8] In the case of multicompositional films, recent reports have indicated that by applying heterojunctions of dissimilar oxides in the form of surface decoration and/or as composites, the gas sensing behavior of resistive sensors is remarkably improved.[9] The main point with heterostructures made by dissimilar oxides is the formation of a depletion layer in the junction. The width of this depletion layer can be changed by the exposed target gas, as a consequence of which conductivity is altered.[10] Moreover, the oxides with different crystal structures as well as nanoparticle size may also lead to an increase in gas adsorption sites on the oxide surface and improve overall performance.[11] Therefore, heterostructures can greatly improve the sensitivity of sensors.

For gas sensing, many studies have also demonstrated that nanomaterials, for example, Si nanowires, are also good sensors.[4,12] They can be easily integrated with CMOS technology, especially in the form of diodes or transistors.[13,14] However, sensors in the form of Si nanowire transistors may show low sensitivity, and the technology used for this purpose is costly and complicated for mass production.[4,15] Therefore,

Received: March 2, 2022
Accepted: April 26, 2022
Published: May 5, 2022

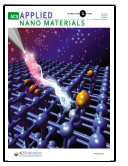

© 2022 The Authors. Published by American Chemical Society

Table 1. Comparative Results of ZnO/SnO_2 Sensors for Gas Sensing

material	concentration (ppm)	response (Ra/Rg)	T (°C)	target gas	ref.
SnO_2/ZnO	0.5	11.5	100	H_2S	6
ZnO/SnO_2	0.5	30	450	H_2S	this paper
SnO_2 promoted with ZnO	0.5	4.5	350	H_2S	41
ZnO/SnO_2 heterogeneous nanospheres	0.5	3.94	300	H_2S	35
SnO_2 promoted with ZnO	0.5	0.71	350	H_2S	42
Au-doped ZnO/SnO_2 nanofibers	1	73.3	350	H_2S	11
ZnO/SnO_2 heterostructure	1	317	350	H_2S	10
SnO_2 nanobowls branched ZnO NWs	1	6.24	250	H_2S	34
CuO functionalized SnO_2–ZnO core–shell NWs	10	1.69	RT	H_2S	43
SnO_2–ZnO core–shell NWs	25	3.08	400	ethanol	44
SnO_2/ZnO hierarchical nanostructures	25	3	400	ethanol	45
ZnO/SnO_2 nanofibers	50	63.3	250	H_2S	46
SnO_2–ZnO core–shell NWs	200	280	400	ethanol	47
SnO_2 doped ZnO	200	40	450–500	ethanol	48

resistive metal oxides are more common sensors because of their simple operation and fabrication technology.[16]

For gas sensing, there are also many applications for medical and safety purposes as well as environmental monitoring requiring robust, compact, and high-performance H_2S gas sensors.[17,18] It is well-known that polluted air contains dangerous gases, for example, O_3, CO_2, CH_a, and CO, where H_2S gas is corrosive and flammable with an infamous rotten egg smell.[11,19] Exposure to even low concentrations of H_2S over a long period of time can cause negative effects on human health such as irritation of the nose, eyes, throat, and respiratory system.[18,20] In addition, identifying H_2S in exhaled breath contributes to the detection of symptoms of a variety of oral diseases such as halitosis.[21]

Nanostructured metal oxides with different morphologies have been utilized for a wide range of applications.[22−25] Among oxide materials, both SnO_2 and ZnO can be easily grown at low temperatures. These oxide materials are commonly used in several sensors for bio and thermal applications. Because low operational temperatures are expected, SnO_2 and ZnO recently attracted widespread attention for use as low-power gas-sensing materials.[26−28] Among metal oxides, heterostructures such as SnO_2/CuO, CuO/ZnO, WO_3/NiO, ZnO/NiO, ZnO/SnO_2, and so on. have been synthesized with different methods as an active material for H_2S gas sensing.[6,29−33] ZnO/SnO_2 sensors show remarkably higher sensitivity than sensors made only from SnO_2 or ZnO under identical experimental conditions.[6] Therefore, this study has chosen to carry out the gas sensing performance of ZnO–SnO_2 materials. In the case of ZnO/SnO_2, for example, Zhu et al. reported well-designed hierarchical and highly-ordered nanobowl ZnO/SnO_2 gas sensors which are sensitive and selective in detecting as low a concentration as 1 ppm H_2S gas with long-term stability and repeatability.[34] The hierarchical sensing materials were synthesized via a sequential process combining hard template processing, atomic-layer deposition, and hydrothermal processing.[34] Furthermore, Guo et al. published a study about the hydrothermal synthesis of ZnO/SnO_2 for H_2S detection.[35] The results revealed that this type of heterostructure has a better H_2S gas response and selectivity among some interfering gases, for example, NO, SO_2, CO, CH_4, and C_2H_5OH.[35] The most important works concerning gas sensing of ZnO/SnO_2 heterostructure are summarized in Table 1.

For metal oxides, the optimum surface temperature for proper interaction with airborne species and sensing is above 300 °C.[36] In order to fabricate such devices, it is required that the metal oxides with a designed texture are deposited on dielectric substrates which are chemically stable at high temperatures.[26] Alumina substrates are widely used for depositing polycrystalline functional metal oxides due to their long list of positive features, including high-temperature stabilities and excellent dielectric properties.[26] Different techniques like molecular beam epitaxy, vapor deposition, pulsed laser ablation, sputtering, ultrasonic spray pyrolysis (USP), electrophoretic deposition, and various sol–gel methods have been utilized for depositing ZnO and SnO_2 on alumina substrates.[37−39] Among these methods, USP provides some degree of control on the microstructure and morphology of the grown layers with a growth rate as high as 100 nm/min.[40] The main advantage of this method is the ability to grow continuous layers that can perfectly follow the shape of the substrate. Besides all these positive features, USP consumes less energy compared to in-vacuum deposition techniques, which makes it more interesting for gas sensing applications.[40]

To the best of our knowledge, this is the first study to demonstrate ZnO/SnO_2 heterostructure grown on alumina substrates using USP deposition for H_2S gas sensing purposes. In this design, the sensing layer is integrated with the heater on the rear of the sensor. The material characterization and gas sensing properties of the grown layers with different ratios of zinc chloride and tin (II) chloride dihydrate in the initial precursor are performed and discussed. The sensing layer's thickness effect on the performance of the sensors is undeniable; however, this research mostly focuses on the heterojunction effect of the sensors. Therefore, the selectivity and gas sensing mechanism of the ZnO/SnO_2 has been systematically investigated.

EXPERIMENTAL SECTION

Alumina plates (3 mm × 3 mm × 0.5 mm) with 99% purity were utilized as substrates. The USP system was utilized to form both a sensing and a heating layer. The details about the USP deposition system have already been presented in our previous work.[26] The substrate temperature of 325 °C was used for all depositions with a precursor spray rate of 4 mL/min. In the first step, the prepared chips were directly placed on the hot stage of the USP system to form microheaters. In the case of the microheater, the precursor solution was prepared by dissolving 0.2 mol/L of $SnCl_2{\cdot}2H_2O$ (23742.260, AnalaR NORMAPUR, VWR) in pure ethanol (99.90% v/v). The

https://doi.org/10.1021/acsanm.2c00940
ACS Appl. Nano Mater. 2022, 5, 6954−6963

Table 2. Details of USP Depositions of Sensing Layers

	S0	S1	S2	S3	S4	S5	S6
$ZnCl_2$:$SnCl_2{\cdot}2H_2O$ precursor solution ratios (V:V)	6:1	5:1	4:2	3:3	2:4	1:5	0:6
deposition time (min)	18.00	13.12	9.00	5.70	5.78	4.80	4.00
measured Zn/Sn ratio from EDX	0.2210	0.1852	0.0998	0.0485	0.0298	0.0258	0

microheater was formed by USP deposition for 75 min on the rear of the sample followed by 1000 °C furnace annealing for an hour (80% N_2 and 20% O_2). For deposition of the sensing layer (on the front of the sample), separate precursor solutions which consist of $ZnCl_2$ (29156.231, AnalaR NORMAPUR, VWR) and $SnCl_2{\cdot}2H_2O$ with a molarity of 0.2 mol/L were prepared using ethanol as solvent. Then different precursor solutions are prepared by mixing a proportional volume of $ZnCl_2$ and $SnCl_2{\cdot}2H_2O$ solutions with the volume ratios as presented in Table 2. Seven samples (S0 to S6) were prepared, among which S6 contained a pure SnO_2 layer and S0 contained the highest investigated amount of $ZnCl_2$. By choosing the appropriate deposition time, the thickness of the sensing layer for all samples was kept the same (130 ± 5 nm). The details of the deposition time for the samples are also presented in Table 2.

The scanning electron microscopy (SEM) (TESCAN MAIA3) tool was utilized to observe the morphology of the grown layers.

The X-ray diffraction (XRD) data were collected in $\theta-2\theta$ and grazing incidence modes by using Cu Kα radiation in a nonfocusing geometry using a Philips X'Pert MRD tool. In order to obtain decent beam intensity and high acquisition, an X-ray mirror was applied in primary optics and a parallel-plate collimator was placed prior to the detector in the secondary optics.

To study the elemental composition and chemical state of the ZnO/SnO_2 heterostructure materials, X-ray photoelectron spectra (XPS) (ESCALAB 250Xi, Thermo Fisher, USA) analysis was carried out in a spectrometer with a monochromatic Al-Kα X-rays source and spot size of 500 μm. All the binding energies were charge corrected by using the C 1s peak at 284.8 eV of the surface contamination carbon. The fitted peaks of O 1s XPS spectra were deconvoluted using an XPS Peak 4.1 software.

The cross-sectional view of ZnO/SnO_2 samples was characterized by transmission electron microscopy (TEM) (Talos F200X, FEI/Thermo Fisher, USA) with an operating voltage of 200 kV. Energy-dispersive X-ray spectroscopy (EDX) was also applied in the TEM tool to determine the element content of ZnO/SnO_2 heterostructure samples. Furthermore, nanobeam electron diffraction and selected area electron diffraction (SAD) were also employed to analyze the phase and crystalline quality in the grain.

Before gas sensing measurements, in order to stabilize the structure of the sensors, 600 °C was chosen to anneal the samples in an air atmosphere for an hour. Figure 1a displays how the prepared gas sensors were mounted on the ceramic support and electrically interconnected to a chip (25 × 35 mm^2) with feedthroughs. Diffusion bonding of 75 μm gold wire was used to make electrical contacts within both heater and sensor structures. The sensors with their chip were mounted inside the closed chamber equipped with mass-flow controllers (see Figure 1b for more details). The cross-sectional SEM micrograph of the SnO_2 heater deposited by the USP technique at 325 °C for 75 min is presented in Figure 1c.

Gas sensing measurements were done using a mass flowmeter and apparatus described in our previous work.[49] The sensor temperature and electrical signal were measured by an s-type thermocouple (Pt and 90%Pt10%Rh wires with 25 μm diameter) and Keithley 2410 electrometer, respectively.

The response calculated according to

$$\text{response} = \frac{I_g - I_a}{I_a} \quad (1)$$

where I_g and I_a are the sensor currents in target gas and atmospheric air, respectively.

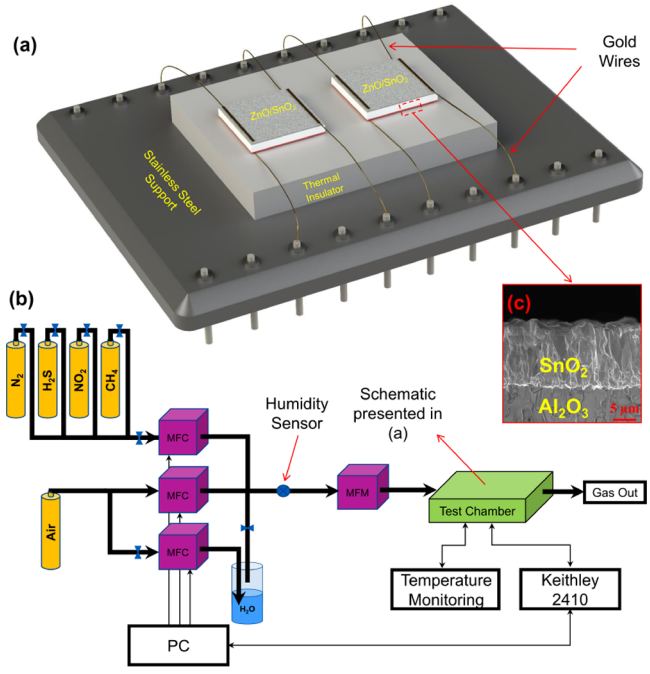

Figure 1. (a) Schematic image of the sample holder, (b) schematic image of the testing set-up, and (c) cross-sectional SEM micrograph of the SnO_2 heater deposited by USP on alumina substrates.

RESULTS AND DISCUSSION

Figure 2 displays the SEM cross-section micrographs (130 ± 5 nm thickness) of ZnO/SnO_2 heterostructure and the corresponding top view plane. The inset images in Figure 2 at higher magnification show the morphology of the grown crystallites. According to our previous work,[26] ZnO crystallites do not grow continuously on alumina substrates, while SnO_2 crystallites perfectly grow on alumina substrates.[26] This behavior also applies to the heterostructure growth of ZnO/SnO_2. This means that for the sensors with a lower amount of $SnCl_2{\cdot}2H_2O$ in the initial precursor, it is necessary to increase the deposition time in order to keep the thickness the same in all sensors. Previously, the effect of thickness on the gas sensing properties of the sensors has already been investigated in detail;[50] however, in this study, the heterojunction effects on gas sensing properties are targeted. Therefore, by changing the deposition time, the thickness of the all sensors was adjusted to be around 130 nm to obtain decent gas sensing measurements.

As observed from the SEM images in Figure 2a–g, with an increase in the $ZnCl_2$ ratio in the precursor the morphology of the grown layers changes slightly. However, thanks to the benefits of USP deposition, the grown crystallites in each sensor have a uniform distribution all over the substrates. In the case of pure SnO_2 (Figure 2a) the nanocrystallites around 57 nm were found on the surface (line averaging was utilized to determine grain size). This number decreased to 47, 50, and 50 nm for the other three sensors (S5, S4, and S3 respectively) as shown in Figure 2b–d. The smallest crystallites (around 35

https://doi.org/10.1021/acsanm.2c00940
ACS Appl. Nano Mater. 2022, 5, 6954–6963

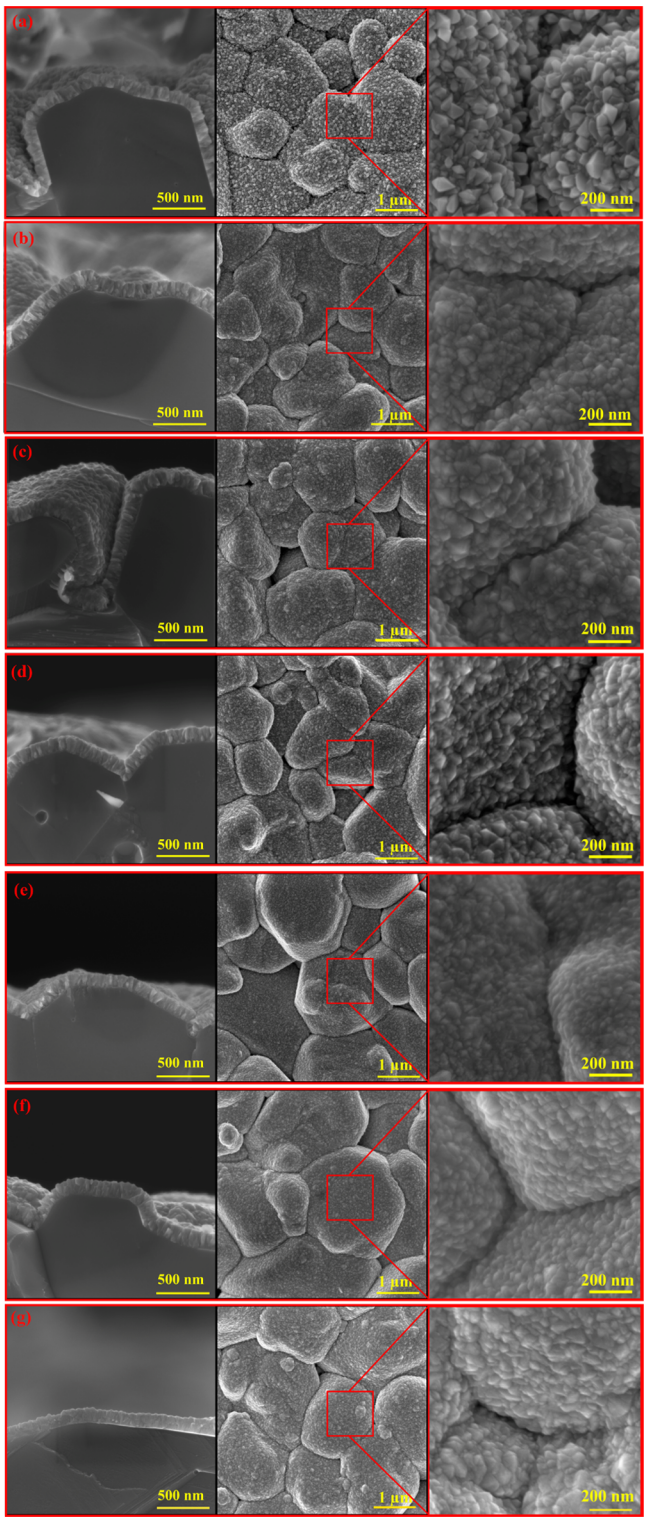

Figure 2. The cross-sectional and plan view SEM micrographs of the sensors prepared by USP at 325 °C on alumina substrates: (a) pure SnO_2 (S6), (b) S5, (c) S4, (d) S3, (e) S2, (f) S1, and (g) S0.

and 39 nm) were found on the surface of S2 and S1, respectively. Then it increased to 49 nm for S0. This result shows that by starting with pure SnO_2 in sample S6 and continuously increasing the $ZnCl_2$ ratio, the size of the crystallites decreases (up to sample S1), and then, it increases (for sample S0). These results are in good agreement with previous reports stating that by introducing Zn atoms to the SnO_2 initial precursor solution, the size of the grown crystallites is affected.[51]

In this part, the crystal structure of the grown layers was studied by applying XRD. Figure 3a illustrates the XRD patterns of our samples. The results reveal that all samples have almost similar XRD characteristics. Apart from the substrate peaks (alumina), there are three distinguishable peaks at 26.6, 33.9, and 51.8° corresponding to the sensor layer. These peaks are indexed to the (110), (101), and (211) of the tetragonal rutile SnO_2 phase.[51] The absence of diffraction peaks of hexagonal ZnO can be due to the relatively small amount of ZnO grown on alumina or to the crystallites being too small to be detected by XRD. Due to the lattice mismatch of the ZnO and SnO_2, it is less likely to dope ZnO crystallites into the SnO_2. Therefore, ZnO crystallites might have been grown in isolation all over the surface, forming an external heterostructure with SnO_2 (more information will be presented later in the XPS part). In spite of the high proportion of $ZnCl_2$ in the initial USP precursor, the highest intensity for (110) reflection of SnO_2 is obtained only for S1. This may also mean that the inclusion of $ZnCl_2$ in the precursor influences the morphology of the film. This may happen because of the slower deposition rate for this sample compared to the other samples. Although the thickness of the layers is the same, deposition time may affect the growth rate of some planes, such as (110). It is important to mention here that there was no detection of any crystalline ternary phases in these layers.

Further study was performed by TEM and EDX to analyze the crystallites of the sensing materials in smaller dimensions and to determine their distribution. Figure 3b shows the bright field (BF), SAD, and EDX images of S1, S3, and S6. In this figure, the SAD image of S1 is only shown because the other samples had a similar feature. The BF images reveal that the material contains mainly crystalline grains but there is a disordered area at the initial stage of the film growth (marked by dashed rings). These phases appear in SAD as concentric rings; meanwhile, there is a hollow ring, which is representative of the disordered region. The rings are identified as planes (110), (101), (111), and (211), which are also consistent with XRD results. There is also a Z-contrast in the BF images where the major distribution of SnO_2 appear brightly and lighter elements such as ZnO are dark regions. There are stacking fault defects in the crystalline grains (marked by arrows). The EDX analysis has been focused on detecting Sn, O, and Zn elements in the samples. The presence of Zn is successively decreased from S1 to S3 until Zn vanishes completely in S6. On closer observation of sample S1, the EDX of Zn appears like bright regions containing small spots, but there are also dark regions without Zn in the layer. The Zn amount in sample S4 is obviously smaller and also nonuniform, like for sample S1.

In order to validate the chemical states and surface elemental composition, XPS measurements of S1 and S6 were carried out. As shown in Figure 4a, the peaks of Zn, Sn, and O, together with C, can be clearly observed in the survey spectrum for S1, whereas peaks of Sn, O, and C are detected for S6, and no other impurities could be observed. The C signal originates mostly from surface hydrocarbons because of the exposure of samples to air or from adventitious hydrocarbons.

As shown in Figure 4b, sample S1 has two strong peaks around 1021.65 and 1044.7 eV in the Zn 2p spectrum. These peaks correspond to Zn 2p 3/2 and Zn 2p 1/2, respectively,

https://doi.org/10.1021/acsanm.2c00940
ACS Appl. Nano Mater. 2022, 5, 6954−6963

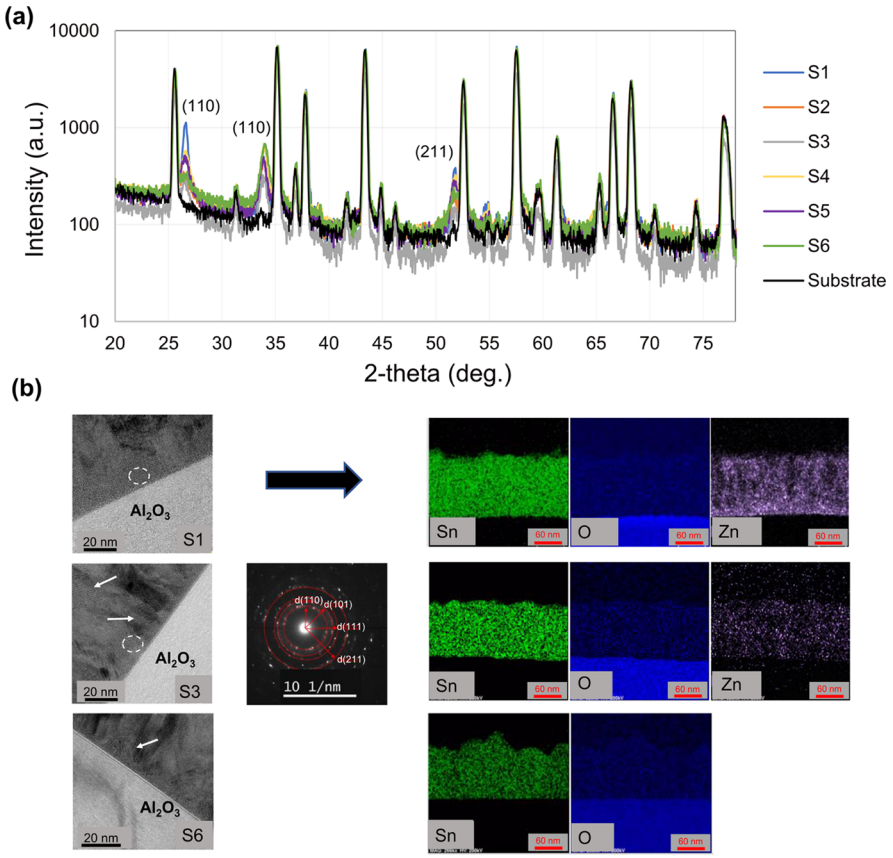

Figure 3. (a) θ–2θ diffractograms from sensors S1 to S6 as well as alumina substrate, and (b) TEM analysis of S1, S3, and S6 samples. The BF, SAD, and EDX images have been illustrated.

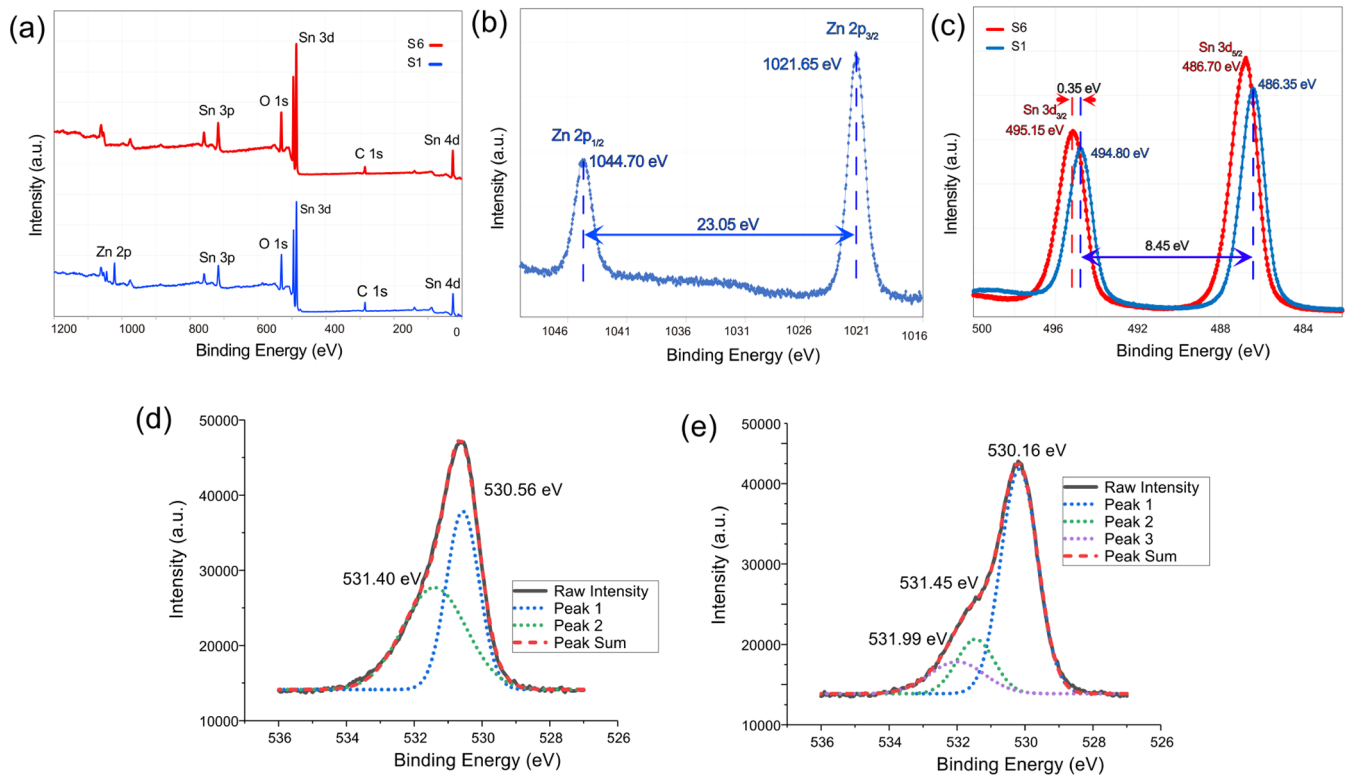

Figure 4. (a) XPS survey spectra of S1(pure SnO_2) and S6 (ZnO/SnO_2). (b) Zn 2p, (c) Sn 3d spectra for S1 and S6. (d) O 1s spectra for S6 and (e) S1.

https://doi.org/10.1021/acsanm.2c00940
ACS Appl. Nano Mater. 2022, 5, 6954–6963

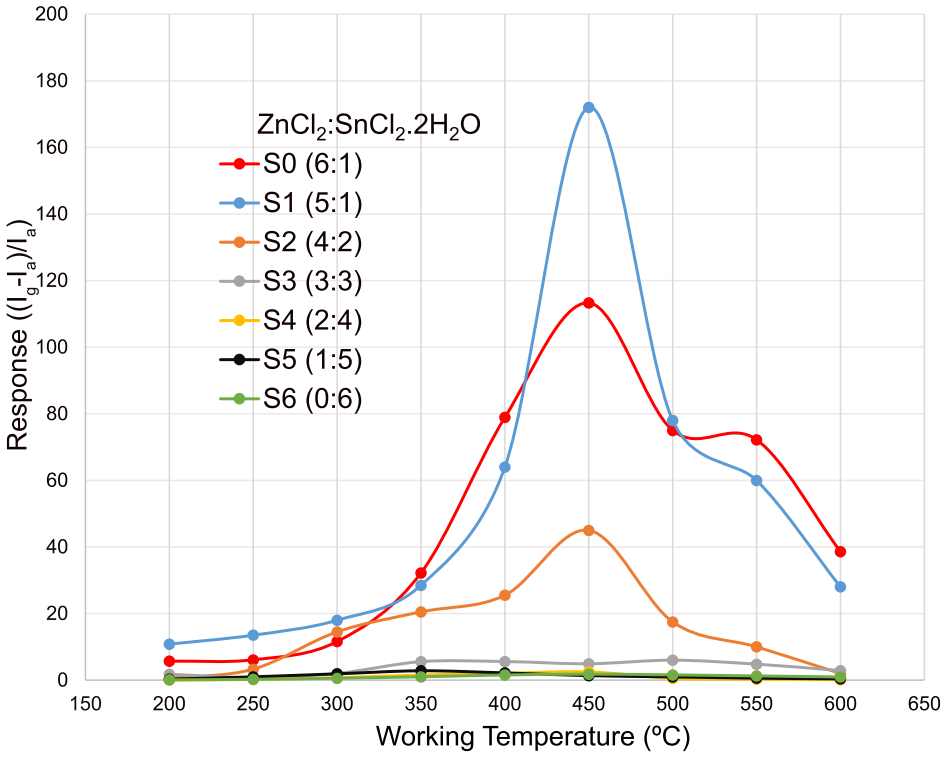

Figure 5. H_2S gas sensing response of the sensors (S1 to S6) as a function of operating temperature.

indicating that the Zn is in the +2 valence state. In addition, the difference in binding energies between them is 23.05 eV; hence, the substance exists in the form of ZnO.[52] The high-resolution spectrum of Sn 3d for sample S6 shows doublet binding energies at 486.70 and 495.15 eV, corresponding to Sn 3d 3/2 and Sn 3d 5/2, respectively, as shown in Figure 4c. The energy difference between doublet binding energies is estimated at 8.45 eV, which is in excellent agreement with the reported values.[51,53] Moreover, the Sn peaks of the S1 composite shift 0.35 eV to lower energies, indicating that the interaction and electron transformation may exist between ZnO and SnO_2 until equilibrium is reached (the same level of Femi energy).[54,55] The Sn 3d XPS peak positions confirm that the oxidation state of the Sn ions is +4 and the difference in binding energy between the two peaks (6.45 eV) indicates that the substance is SnO_2, which is in good agreement with XRD analysis.

Oxygen species play an important role in the gas sensing ability of the sensors by changing the thickness of the depletion layer. Due to the asymmetric shape of the O 1s spectrum in both S1 and S6, it can be deconvoluted into different symmetric peaks to verify the status of oxygen species. For S6 (SnO_2), according to Figure 4d, O 1s can be deconvoluted into nearly two peaks at binding energies of 530.56 and 531.4 eV. The lower binding energy corresponds to the oxygen atoms located in the lattice in the form of Sn−O. The peak at 531.4 eV could be ascribed to the oxygen vacancies in the structure of regular rutile SnO_2. In the case of S1 (ZnO/SnO_2) O 1s can be deconvoluted into three peaks as shown in Figure 4e. The lower binging energy at 530.16 eV is attributed to the lattice oxygens in the form of Zn−O and Sn−O. The second binding energy at 531.45 eV is ascribed to the oxygen vacancies in the ZnO/SnO_2 structure. The highest binding energy located at 531.99 eV is related to the oxygen atoms chemisorbed at the surface of synthesized materials. This indicates that the ability of chemisorbing of oxygen on the surface of S1 (ZnO/SnO_2) is remarkably stronger than single component SnO_2. Therefore, the surface oxygen adsorption ability of the sensor greatly contributes to the capability of reacting with target gas molecules and it has the potential to perform well as a gas sensing material.[56]

The response of a gas sensor is remarkably affected by the operating temperature. Hence, the relationship between the gas sensing response and the operating temperature was first investigated in Figure 5, where all sensors are exposed to 5 ppm of H_2S at different operating temperatures ranging from 200 to 600 °C. For sensors S3 to S6, the response is measured to be less than six according to eq 1 at all operating temperatures. For sensors S0, S1, and S2, their gas sensing responses continued to grow as the operating temperature increased from 200 to 450 °C. The maximum amount of response was obtained at 450 °C (113, 172, and 45 for S0, S1, and S2, respectively), indicating that the optimal operating temperature for this designed material combination could be chosen as 450 °C and the most sensitive sensor is S1. For this operating temperature the response and recovery time are 37, and 57 s, respectively. However, all the responses began to decrease as the operating temperature further increased above 450 °C (up to 600 °C). Basically, certain activation energy is required to have a reaction between the target gas and adsorbed oxygen species. At low operating temperatures, gas molecules are not activated enough to overcome the activation energy barrier to react with oxygen species on the surface of ZnO/SnO_2 which leads to low response and longer response and recovery time. By increasing the temperature, the conversion of surface-adsorbed oxygen species and higher reaction activity contribute to the higher response. By increasing the temperature above the operating temperature, H_2S gas adsorption is too difficult to be adequately compensated for the increased surface reactivity which causes

https://doi.org/10.1021/acsanm.2c00940
ACS Appl. Nano Mater. 2022, 5, 6954−6963

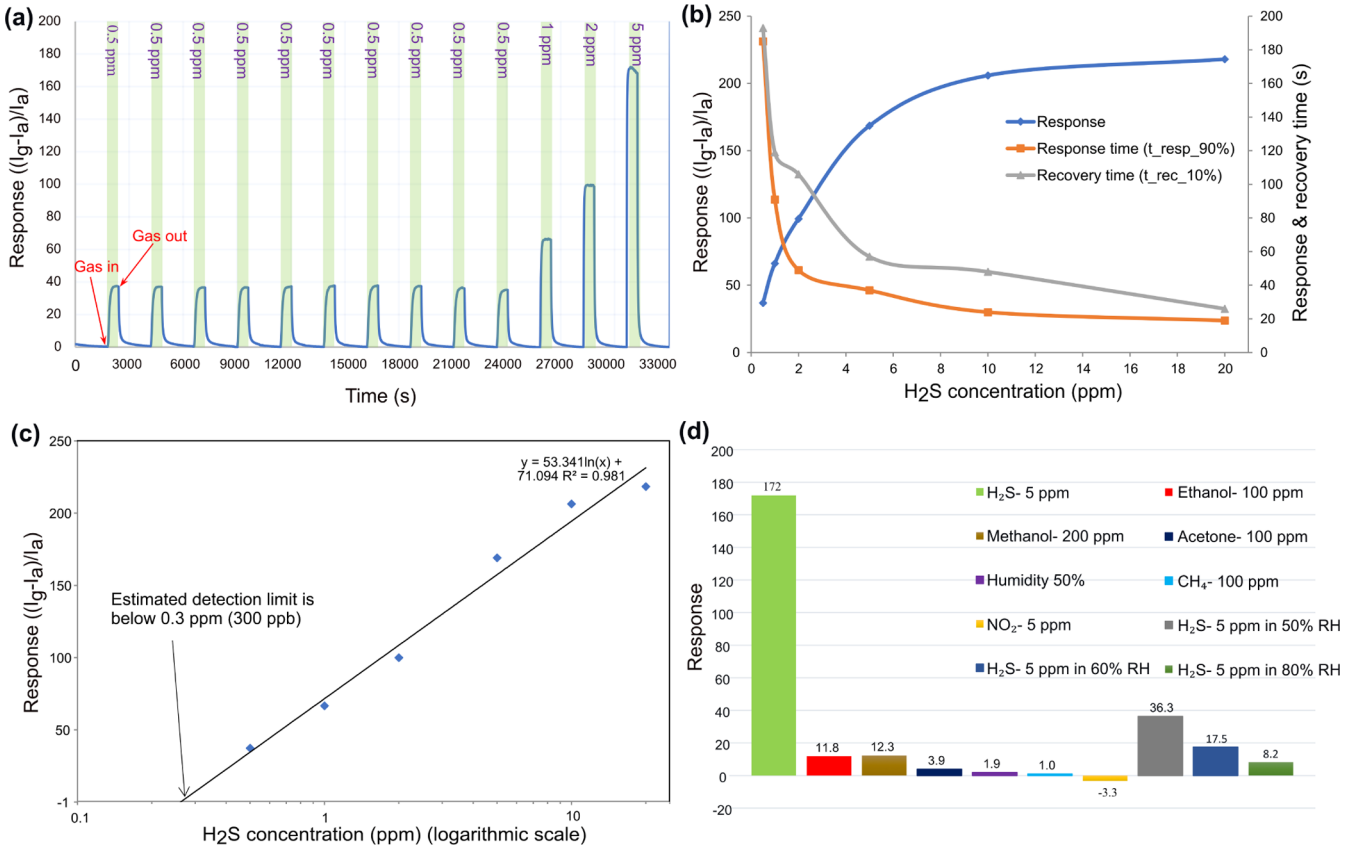

Figure 6. (a) Dynamic response curve of the S1 sensor for H_2S gas with concentrations ranging from 0.5 to 5 ppm at 450 °C operating temperature. (b) Response and recovery time versus concentration, and (c) Prediction for the low detection limit of the sensor. (d) Response of S1 toward 5 ppm of H_2S and some other interfering gases with higher concentrations.

a low utilization rate of the sensing material.[57] In addition, at higher operating temperatures the response and recovery time are shorter, but the response is lower, and because of the higher operating temperature, more energy has to be consumed. In this work, sensor S1 displayed the highest response at 450 °C, which may be closely related to both the establishment of heterostructure and the effective increase in the specific surface area for oxygen adsorption.

Figure 6a shows the corresponding dynamic gas sensing response curves of the S1 (ZnO/SnO_2) sensor at the optimal operating temperature of 450 °C, for various H_2S concentrations ranging from 0.5 to 20 ppm. The obtained sensing response values are about 37, 66, 99, 172, 206, and 218 for 0.5, 1, 2, 5, 10, and 20 ppm H_2S, respectively (see Figure 6b). There is a small drop in the signal for 5 ppm and this drop can be attributed to the saturation levels of different materials that we have in the heterostructure (SnO_2 and ZnO). This saturation of the sensor starts at 5 ppm as can be observed from Figure 6b (blue line). This sensor could recover to its initial value when exposed to air again, implying satisfactory stability and reproducibility of the proposed H_2S gas sensor. All the response times and recovery times for different concentrations of target gas are presented in Figure 6b. The repeatability of the fabricated ZnO/SnO_2 (S1) sensor was measured to 0.5 ppm H_2S gas at 450 °C 10 times as shown at the beginning of the dynamic response in Figure 6a (response: 36.25 ± 1.25). The measured results indicate that the response has little change. This confirms the good stability of the fabricated ZnO/SnO_2 (S1) sensor. In addition, the long-term stability of the sensor over 30 days is presented in Figure S2. To estimate the limit of the detection (LoD) of S1 the calibration curve was prepared for the concentration range of 0.5−20 ppm (Figure 6d—blue line and Figure 6c in the logarithmic scale). The data were fitted using the logarithmic fitting (least squares method where the concentration values were logarithm), the fitted curve and its equation are presented in Figure 6c. Then the fitted line was used to extrapolate its intersection with the doubled noise level (response value of 1), this LoD is lower than 0.3 ppm of H_2S.

The response actions of ZnO/SnO_2 of the S1 sensor for six different gases are shown in Figure 6d. It can be seen that the highest response of the S1 sensor is observed for 5 ppm H_2S sensing, which is almost 14 times higher than methanol, ethanol, and some other gases (with higher concentration levels, see the dynamic responses for these gases at Supporting Information, Figure S1). The reason behind the selectivity of ZnO/SnO_2 can be attributed to the relatively small molecular size of H_2S among most of the gases, which leads it to possess a larger adsorption capacity on the same surface adsorption area.[34] In another work from Fu. et al. demonstrated that ZnO will react with H_2S and transfer to ZnS leading to a larger response because the conductivity of ZnS is higher than that of ZnO.[6] The abovementioned results demonstrate that the ZnO/SnO_2 sensor S1 can be used for H_2S detection. However, humidity has a negative effect on the sensor's response. In order to have more information, sensor S1 was exposed to 5 ppm of H_2S within relative humidity levels of 50, 60, and 80%. As presented in Figure 6d, the sensor's responses are 36.3,

https://doi.org/10.1021/acsanm.2c00940
ACS Appl. Nano Mater. 2022, 5, 6954−6963

17.5, and 8.2 respectively. This means that future works are required to improve the performance of the sensor in humid conditions.

The gas-sensing mechanism of ZnO/SnO_2 heterostructures could be described by the surface depletion and grain boundary mechanism. The gas response of the sensor in pure SnO_2 can be originated from the homojunction barrier of the intergranular barrier in SnO_2.[20] In the air atmosphere, the adsorption of oxygen molecules in the form of O_2^-, O^-, and O^{2-} generates an electron depletion layer at the surface, resulting in a decrease in conductivity.[4] Upon exposure to the target gas, the reaction between H_2S molecules and oxygen preadsorbed species on the surface of SnO_2 can return electrons to the conduction band.[10] This decreases the width of the depletion layer and increases conductivity. In the case of ZnO/SnO_2 heterostructure, the sensitivity is higher than the pure SnO_2. This behavior is mainly attributed to the heterojunctions between ZnO and SnO_2.[35] When dissimilar semiconducting materials, for example, SnO_2 and ZnO, which have different Fermi levels, are brought into contact, the electrons from SnO_2 with lower work function (Φ = 4.9 eV) transfer across the interface to ZnO with higher work function (Φ = 5.2 eV) until the Fermi levels are equilibrated.[45] As a result, band bending and charge distribution happen at the interface of the junction. Consequently, the accumulation layer is formed on the ZnO side and a depletion layer is created on the SnO_2 side. In order to have any conduction in the sensing material, the charge carriers have to overcome this potential barrier.[45] Upon exposure to the air atmosphere, electrons are extracted from the conduction band of ZnO and SnO_2, and consequently, the potential barrier between ZnO and SnO_2 increases. When this junction is exposed to the H_2S gas, the potential barrier decreases.[34] Herein, this junction plays a critical role in enhancing the gas response of the sensor.

CONCLUSIONS

Novel gas sensors made of ZnO/SnO_2 materials on alumina substrates with high sensitivity for sensing the H_2S gas within an operating temperature range of 200−650 °C have been presented. A heater has been also integrated into the rear of the sensor for raising the operating temperature. The performance of the sensing material was improved by optimizing the solution ratios made of zinc chloride and tin (II) chloride dihydrate. The sensor with 5:1 ($ZnCl_2$: $SnCl_2 \cdot 2H_2O$) ratio in the USP precursor exhibited ∼95 times better response than the pure SnO_2 sensor toward 5 ppm H_2S at the operating temperature of 450 °C. The enhanced gas-sensing performance was due to the heterostructure formation between ZnO and SnO_2. The main advantage of the sensor is its inexpensive one-step USP-based fabrication process on alumina substrate and its relatively high sensitivity in the range of single ppm and sub-ppm concentrations of H_2S without any additional functionalization. Other advantages are the integrated heating element on the rear of the sensor made with a similar process (USP) and possible miniaturization of the sensing structure for future improvement of sensor power consumption. Based on our results, the simple ZnO/SnO_2 heterostructures made by USP are good candidates for improved selective and sensitive H_2S detection.

ASSOCIATED CONTENT

Supporting Information

The Supporting Information is available free of charge at https://pubs.acs.org/doi/10.1021/acsanm.2c00940.

Dynamic responses of S1 to ethanol, NO_2, methane, methanol, and acetone and long term stability of S1 over 30 days (PDF)

AUTHOR INFORMATION

Corresponding Authors

Mehdi Akbari-Saatlu − *Department of Electronics Design, Mid Sweden University, Sundsvall SE-85170, Sweden;* orcid.org/0000-0003-2602-7634; Email: mehdiakbari125@gmail.com, mehdi.akbarisaatlu@miun.se

Wenjuan Xiong − *Key Laboratory of Microelectronic Devices & Integrated Technology, Institute of Microelectronics, Chinese Academy of Sciences, Beijing 100029, People's Republic of China*; Email: xiongwenjuan@ime.ac.cn

Henry H. Radamson − *Department of Electronics Design, Mid Sweden University, Sundsvall SE-85170, Sweden; Guangdong Greater Bay Area Institute of Integrated Circuit and System, Guangzhou 510535, China; Key Laboratory of Microelectronic Devices & Integrated Technology, Institute of Microelectronics, Chinese Academy of Sciences, Beijing 100029, People's Republic of China*; Email: Henry.Radamson@miun.se

Authors

Marcin Procek − *Department of Electronics Design, Mid Sweden University, Sundsvall SE-85170, Sweden; Department of Optoelectronics, Silesian University of Technology, Gliwice 44-100, Poland*

Claes Mattsson − *Department of Electronics Design, Mid Sweden University, Sundsvall SE-85170, Sweden*

Göran Thungström − *Department of Electronics Design, Mid Sweden University, Sundsvall SE-85170, Sweden*

Tobias Törndahl − *Department of Materials Science and Engineering, Ångström Laboratory, Uppsala University, Uppsala SE-75103, Sweden;* orcid.org/0000-0001-7757-5847

Ben Li − *Guangdong Greater Bay Area Institute of Integrated Circuit and System, Guangzhou 510535, China*

Jiale Su − *Guangdong Greater Bay Area Institute of Integrated Circuit and System, Guangzhou 510535, China; Key Laboratory of Microelectronic Devices & Integrated Technology, Institute of Microelectronics, Chinese Academy of Sciences, Beijing 100029, People's Republic of China*

Complete contact information is available at: https://pubs.acs.org/10.1021/acsanm.2c00940

Funding

This work has been founded by EU regional fund and Swedish innovation agency (Vinnova).

Notes

The authors declare no competing financial interest.

REFERENCES

(1) Wang, J.; Shen, H.; Xia, Y.; Komarneni, S. Light-Activated Room-Temperature Gas Sensors Based on Metal Oxide Nanostructures: A Review on Recent Advances. *Ceram. Int.* **2021**, *47*, 7353−7368.

(2) Comini, E. Metal Oxides Nanowires Chemical/Gas Sensors: Recent Advances. *Mater. Today Adv.* **2020**, *7*, 100099.
(3) Mirzaei, A.; Lee, J.-H.; Majhi, S. M.; Weber, M.; Bechelany, M.; Kim, H. W.; Kim, S. S. Resistive Gas Sensors Based on Metal-Oxide Nanowires. *J. Appl. Phys.* **2019**, *126*, 241102.
(4) Akbari-Saatlu, M.; Procek, M.; Mattsson, C.; Thungström, G.; Nilsson, H.-E.; Xiong, W.; Xu, B.; Li, Y.; Radamson, H. H. Silicon Nanowires for Gas Sensing: A Review. *Nanomaterials* **2020**, *10*, 2215.
(5) Zhang, D.; Yang, Z.; Yu, S.; Mi, Q.; Pan, Q. Diversiform Metal Oxide-Based Hybrid Nanostructures for Gas Sensing with Versatile Prospects. *Coord. Chem. Rev.* **2020**, *413*, 213272.
(6) Fu, D.; Zhu, C.; Zhang, X.; Li, C.; Chen, Y. Two-Dimensional Net-like SnO2/ZnO Heteronanostructures for High-Performance H2S Gas Sensor. *J. Mater. Chem. A* **2016**, *4*, 1390−1398.
(7) Walker, J. M.; Akbar, S. A.; Morris, P. A. Synergistic Effects in Gas Sensing Semiconducting Oxide Nano-Heterostructures: A Review. *Sens. Actuators, B* **2019**, *286*, 624−640.
(8) Zappa, D.; Galstyan, V.; Kaur, N.; Munasinghe Arachchige, H. M. M.; Sisman, O.; Comini, E. "Metal Oxide -Based Heterostructures for Gas Sensors"- A Review. *Anal. Chim. Acta* **2018**, *1039*, 1−23.
(9) Yang, S.; Lei, G.; Xu, H.; Lan, Z.; Wang, Z.; Gu, H. Metal Oxide Based Heterojunctions for Gas Sensors: A Review. *Nanomater* **2021**, *11*, 1026.
(10) Phuoc, P. H.; Viet, N. N.; Thong, L. V.; Hung, C. M.; Hoa, N. D.; Duy, N. V.; Hong, H. S.; Hieu, N. V. Comparative study on the gas-sensing performance of ZnO/SnO2 external and ZnO-SnO2 internal heterojunctions for ppb H2S and NO2 gases detection. *Sens. Actuators, B* **2021**, *334*, 129606.
(11) Hung, C. M.; Phuong, H. V.; Van Thinh, V.; Hong, L. T.; Thang, N. T.; Hanh, N. H.; Dich, N. Q.; Van Duy, N.; Van Hieu, N.; Hoa, N. D. Au Doped ZnO/SnO2 Composite Nanofibers for Enhanced H2S Gas Sensing Performance. *Sens. Actuators, A* **2021**, *317*, 112454.
(12) Radamson, H. H.; Zhu, H.; Wu, Z.; He, X.; Lin, H.; Liu, J.; Xiang, J.; Kong, Z.; Xiong, W.; Li, J.; Cui, H.; Gao, J.; Yang, H.; Du, Y.; Xu, B.; Li, B.; Zhao, X.; Yu, J.; Dong, Y.; Wang, G. State of the Art and Future Perspectives in Advanced CMOS Technology. *Nanomaterials* **2020**, *10*, 1555.
(13) Zhang, P.; Xiao, Y.; Zhang, J.; Liu, B.; Ma, X.; Wang, Y. Highly Sensitive Gas Sensing Platforms Based on Field Effect Transistor-A Review. *Anal. Chim. Acta* **2021**, *1172*, 338575.
(14) Radamson, H. H.; Luo, J.; Simoen, E.; Zhao, C. *CMOS Past, Present and Future*; Elsevier, 2018.
(15) Li, Y.; Wang, G.; Akbari-Saatlu, M.; Procek, M.; Radamson, H. H. Si and SiGe Nanowire for Micro-Thermoelectric Generator: A Review of the Current State of the Art. *Front. Mater.* **2021**, *8*, 78.
(16) Al-Hashem, M.; Akbar, S.; Morris, P. Role of Oxygen Vacancies in Nanostructured Metal-Oxide Gas Sensors: A Review. *Sens. Actuators, B* **2019**, *301*, 126845.
(17) Mirzaei, A.; Kim, S. S.; Kim, H. W. Resistance-Based H2S Gas Sensors Using Metal Oxide Nanostructures: A Review of Recent Advances. *J. Hazard. Mater.* **2018**, *357*, 314−331.
(18) Yang, S.; Sun, J.; Xu, L.; Zhou, Q.; Chen, X.; Zhu, S.; Dong, B.; Lu, G.; Song, H. Au@ZnO functionalized three-dimensional macroporous WO3: A application of selective H2S gas sensor for exhaled breath biomarker detection. *Sens. Actuators, B* **2020**, *324*, 128725.
(19) Phuoc, P. H.; Hung, C. M.; Van Toan, N.; Van Duy, N.; Hoa, N. D.; Van Hieu, N. One-Step Fabrication of SnO2 Porous Nanofiber Gas Sensors for Sub-Ppm H2S Detection. *Sens. Actuators, A* **2020**, *303*, 111722.
(20) Hossein-Babaei, F.; Masoumi, S.; Aghili, S.; Shokrani, M. Atmospheric Dependence of Thermoelectric Generation in SnO2 Thin Films with Different Intergranular Potential Barriers Utilized for Self-Powered H2S Sensor Fabrication. *ACS Appl. Electron. Mater.* **2021**, *3*, 353−361.
(21) Lee, I.; Choi, S.-J.; Park, K.-M.; Lee, S. S.; Choi, S.; Kim, I.-D.; Park, C. O. The Stability, Sensitivity and Response Transients of ZnO, SnO2 and WO3 Sensors under Acetone, Toluene and H2S Environments. *Sens. Actuators, B* **2014**, *197*, 300−307.
(22) Hossein-Babaei, F.; Yousefiazari, E.; Ghalamboran, M. Pressure Sensitivity of Charge Conduction Through the Interface Between a Metal Oxide Nanocrystallite and Graphene. *Adv. Mater. Interfaces* **2021**, *8*, 2001815.
(23) Mahdavi, H.; Rahbarpour, S.; Hosseini-Golgoo, S.-M.; Jamaati, H. Reducing the Destructive Effect of Ambient Humidity Variations on Gas Detection Capability of a Temperature Modulated Gas Sensor by Calcium Chloride. *Sens. Actuators, B* **2021**, *331*, 129091.
(24) Procek, M.; Stolarczyk, A.; Pustelny, T. Impact of Temperature and UV Irradiation on Dynamics of NO2 Sensors Based on ZnO Nanostructures. *Nanomater* **2017**, *7*, 312.
(25) Hossein-Babaei, F.; Alaei-Sheini, N.; Jahangiri, M. The Ohmic Contact between Zinc Oxide and Highly Oriented Pyrolytic Graphite. *Mater. Lett.* **2017**, *192*, 52−55.
(26) Hossein-Babaei, F.; Akbari-Saatlu, M. Growing Continuous Zinc Oxide Layers with Reproducible Nanostructures on the Seeded Alumina Substrates Using Spray Pyrolysis. *Ceram. Int.* **2020**, *46*, 8567−8574.
(27) Kang, Y.; Yu, F.; Zhang, L.; Wang, W.; Chen, L.; Li, Y. Review of ZnO-Based Nanomaterials in Gas Sensors. *Solid State Ionics* **2021**, *360*, 115544.
(28) Das, S.; Jayaraman, V. SnO2: A Comprehensive Review on Structures and Gas Sensors. *Prog. Mater. Sci.* **2014**, *66*, 112−255.
(29) Fan, C.; Sun, F.; Wang, X.; Majidi, M.; Huang, Z.; Kumar, P.; Liu, B. Enhanced H2S Gas Sensing Properties by the Optimization of P-CuO/n-ZnO Composite Nanofibers. *J. Mater. Sci.* **2020**, *5518*, 7702−7714.
(30) Wei, Z.; Zhou, Q.; Zeng, W. Hierarchical WO3-NiO microflower for high sensitivity detection of SF6 decomposition byproduct H2S. *Nanotechnology* **2020**, *31*, 215701.
(31) Park, K.-R.; Cho, H.-B.; Lee, J.; Song, Y.; Kim, W.-B.; Choa, Y.-H. Design of Highly Porous SnO2-CuO Nanotubes for Enhancing H2S Gas Sensor Performance. *Sens. Actuators, B* **2020**, *302*, 127179.
(32) Qu, Z.; Fu, Y.; Yu, B.; Deng, P.; Xing, L.; Xue, X. High and Fast H2S Response of NiO/ZnO Nanowire Nanogenerator as a Self-Powered Gas Sensor. *Sens. Actuators, B* **2016**, *222*, 78−86.
(33) Al-Jumaili, H. S.; Jasim, M. N. PREPARATION AND CHARACTERIZATION OF ZnO: SnO 2 NANOCOMPOSITE THIN FILMS ON POROUS SILICON AS H 2 S GAS SENSOR. *J. Ovonic Res.* **2019**, *15*, 81−87.
(34) Zhu, L.-Y.; Yuan, K.-P.; Yang, J.-H.; Hang, C.-Z.; Ma, H.-P.; Ji, X.-M.; Devi, A.; Lu, H.-L.; Zhang, D. W. Hierarchical Highly Ordered SnO2 Nanobowl Branched ZnO Nanowires for Ultrasensitive and Selective Hydrogen Sulfide Gas Sensing. *Microsyst. Nanoeng.* **2020**, *6*, 1−13.
(35) Guo, W.; Mei, L.; Wen, J.; Ma, J. High-Response H2S Sensor Based on ZnO/SnO2 Heterogeneous Nanospheres. *RSC Adv.* **2016**, *6*, 15048−15053.
(36) Jian, Y.; Hu, W.; Zhao, Z.; Cheng, P.; Haick, H.; Yao, M.; Wu, W. Gas Sensors Based on Chemi-Resistive Hybrid Functional Nanomaterials. *Nano-Micro Lett.* **2020**, *12*, 1−43.
(37) Khan, M. A. H.; Rao, M. V.; Li, Q. Recent Advances in Electrochemical Sensors for Detecting Toxic Gases: NO2, SO2 and H2S. *Sensors* **2019**, *19*, 905.
(38) Hossein-Babaei, F.; Ghalamboran, M.; Yousefiazari, E. Electrophoretic Deposition of ZnO on Highly Oriented Pyrolytic Graphite Substrates. *Mater. Lett.* **2017**, *209*, 404−407.
(39) Kumar, R.; Liu, X.; Zhang, J.; Kumar, M. Room-Temperature Gas Sensors Under Photoactivation: From Metal Oxides to 2D Materials. *Nano-Micro Lett.* **2020**, *12*, 1−37.
(40) Hossein-Babaei, F.; Akbari-Saatlu, M. Growth of ZnO Nanorods on the Surface and Edges of a Multilayer Graphene Sheet. *Scr. Mater.* **2017**, *139*, 77−82.
(41) Hwang, B. W.; Lee, S. C.; Ahn, J. H.; Kim, S. Y.; Jung, S. Y.; Lee, D. D.; Huh, J. S.; Kim, J. C. High Sensitivity and Recoverable SnO2-Based Sensor Promoted with Fe2O3 and ZnO for Sub-Ppm H2S Detection. *J. Nanoelectron. Optoelectron.* **2017**, *12*, 617−621.
(42) Lee, S. C.; Kim, S. Y.; Hwang, B. W.; Jung, S. Y.; Lee, S. U.; Lee, D. D.; Kim, J. C. New SnO2-Based Gas Sensor Promoted with

https://doi.org/10.1021/acsanm.2c00940
ACS Appl. Nano Mater. 2022, 5, 6954−6963

ZnO and MoO3 for the Detection of H2S. *Sens. Lett.* **2014**, *12*, 1181−1185.
(43) Kim, J.-H.; Mirzaei, A.; Bang, J. H.; Kim, H. W.; Kim, S. S. Selective H2S Sensing without External Heat by a Synergy Effect in Self-Heated CuO-Functionalized SnO2-ZnO Core-Shell Nanowires. *Sens. Actuators, B* **2019**, *300*, 126981.
(44) Thanh Le, D. T.; Trung, D. D.; Chinh, N. D.; Thanh Binh, B. T.; Hong, H. S.; Van Duy, N.; Hoa, N. D.; Van Hieu, N. Facile synthesis of SnO2-ZnO core-shell nanowires for enhanced ethanol-sensing performance. *Curr. Appl. Phys.* **2013**, *13*, 1637−1642.
(45) Khoang, N. D.; Trung, D. D.; Van Duy, N.; Hoa, N. D.; Van Hieu, N. Design of SnO2/ZnO Hierarchical Nanostructures for Enhanced Ethanol Gas-Sensing Performance. *Sens. Actuators, B* **2012**, *174*, 594−601.
(46) Lu, Z.; Zhou, Q.; Wang, C.; Wei, Z.; Xu, L.; Gui, Y. Electrospun ZnO-SnO2 Composite Nanofibers and Enhanced Sensing Properties to SF6 Decomposition Byproduct H2S. *Front. Chem.* **2018**, *6*, 540.
(47) Hwang, I.-S.; Kim, S.-J.; Choi, J.-K.; Choi, J.; Ji, H.; Kim, G.-T.; Cao, G.; Lee, J.-H. Synthesis and gas sensing characteristics of highly crystalline ZnO-SnO2 core-shell nanowires. *Sens. Actuators, B* **2010**, *148*, 595−600.
(48) Nanto, H.; Morita, T.; Habara, H.; Kondo, K.; Douguchi, Y.; Minami, T. Doping Effect of SnO2 on Gas Sensing Characteristics of Sputtered ZnO Thin Film Chemical Sensor. *Sens. Actuators, B* **1996**, *36*, 384−387.
(49) Akbari-Saatlu, M.; Procek, M.; Thungstrom, G.; Mattsson, C.; Radamson, H. H. H2S Gas Sensing Based on SnO2 Thin Films Deposited by Ultrasonic Spray Pyrolysis on Al2O3 Substrate. *2021 IEEE Sensors Appl. Symp. SAS 2021 - Proc*; IEEE, 2021.
(50) Hossein-Babaei, F.; Orvatinia, M. Analysis of Thickness Dependence of the Sensitivity in Thin Film Resistive Gas Sensors. *Sens. Actuators, B* **2003**, *89*, 256−261.
(51) Li, W.; Ma, S.; Li, Y.; Yang, G.; Mao, Y.; Luo, J.; Gengzang, D.; Xu, X.; Yan, S. Enhanced ethanol sensing performance of hollow ZnO-SnO2 core-shell nanofibers. *Sens. Actuators, B* **2015**, *211*, 392−402.
(52) Hu, K.; Wang, F.; Shen, Z.; Liu, H.; Xiong, J. Ternary heterojunctions synthesis and sensing mechanism of Pd/ZnO-SnO2 hollow nanofibers with enhanced H2 gas sensing properties. *J. Alloys Compd.* **2021**, *850*, 156663.
(53) Hu, K.; Wang, F.; Yan, Y.; Liu, H.; Shen, Z. One Step from Nanofiber to Functional Hybrid Structure: Pd Doped ZnO/SnO2 Heterojunction Nanofibers with Hexagonal ZnO Columns for Enhanced Low-Temperature Hydrogen Gas Sensing. *Ceram. Int.* **2021**, *47*, 15228−15236.
(54) Bai, S.; Fu, H.; Zhao, Y.; Tian, K.; Luo, R.; Li, D.; Chen, A. On the Construction of Hollow Nanofibers of ZnO-SnO2 Hetero-junctions to Enhance the NO2 Sensing Properties. *Sens. Actuators, B* **2018**, *266*, 692−702.
(55) Zheng, X.; Fan, H.; Wang, H.; Yan, B.; Ma, J.; Wang, W.; Yadav, A. K.; Dong, W.; Wang, S. ZnO-SnO2 nano-heterostructures with high-energy facets for high selective and sensitive chlorine gas sensor. *Ceram. Int.* **2020**, *46*, 27499−27507.
(56) Liu, J.; Wang, T.; Wang, B.; Sun, P.; Yang, Q.; Liang, X.; Song, H.; Lu, G. Highly Sensitive and Low Detection Limit of Ethanol Gas Sensor Based on Hollow ZnO/SnO2 Spheres Composite Material. *Sens. Actuators, B* **2017**, *245*, 551−559.
(57) Zhang, Y.; Zeng, W.; Li, Y. The Hydrothermal Synthesis of 3D Hierarchical Porous MoS2 Microspheres Assembled by Nanosheets with Excellent Gas Sensing Properties. *J. Alloys Compd.* **2018**, *749*, 355−362.

NOTE ADDED AFTER ASAP PUBLICATION

A correction was made in the Conclusions to the sentence beginning, The sensor with..., on May 5, 2022.

Recommended by ACS

Pt Nanoparticle-Modified SnO_2–ZnO Core–Shell Nanosheets on Microelectromechanical Systems for Enhanced H_2S Detection
Xue-Yan Wu, Hong-Liang Lu, *et al.*
APRIL 20, 2022
ACS APPLIED NANO MATERIALS
READ

Nanostructured Indium Oxide Thin Films as a Room Temperature Toluene Sensor
Sunil Gavaskar Dasari, Ramana Reddy M V, *et al.*
JULY 01, 2021
ACS OMEGA
READ

Water-Selective Nanostructured Dehumidifiers for Molecular Sensing Spaces
Jiangyang Liu, Takeshi Yanagida, *et al.*
JANUARY 24, 2022
ACS SENSORS
READ

ZnO Nanorods with Doubly Positive Oxygen Vacancies for Efficient Xylene Sensing
Hui Yang, Le-Xi Zhang, *et al.*
FEBRUARY 19, 2022
ACS APPLIED NANO MATERIALS
READ

Get More Suggestions >

https://doi.org/10.1021/acsanm.2c00940
ACS Appl. Nano Mater. 2022, 5, 6954−6963